Supporting Information for

# High Performance $Rh_2P$ Electrocatalyst for Efficient Water Splitting

Haohong Duan,[†,‡,▽] Dongguo Li,[§,▽] Yan Tang,[∥,▽] Yang He,[⊥] Shufang Ji,[†] Rongyue Wang,[§] Haifeng Lv,[§] Pietro P. Lopes,[§] Arvyd as P. Paulikas,[§] Haoyi Li,[∥] Scott X. Mao,[⊥] Chongmin Wang,[#] Nenad M. Markovic,[§] Jun Li,[*,∥] Vojislav R. Stamenkovic[*,§] and Yadong Li[*,†]

[†]Department of Chemistry and Collaborative Innovation Center for Nanomaterial Science and Engineering, Tsinghua University, Beijing 100084, China

[‡]Chemistry Research Laboratory, Department of Chemistry, University of Oxford, 12 Mansfield Road, Oxford, OX1 3TA, UK.

[§]Argonne National Laboratory, Materials Science Divisions, Lemont, IL 60439, United States

[∥]Department of Chemistry and Key Laboratory of Organic Optoelectronics & Molecular Engineering of Ministry of Education, Tsinghua University, Beijing 100084, China

[⊥]Department of Mechanical Engineering and Materials Science, University of Pittsburgh, Pittsburgh, PA 15261, USA

[#]Environmental Molecular Sciences Laboratory, Pacific Northwest National Laboratory, Richland, WA 99352, USA

**Corresponding Authors:**

[*]junli@tsinghua.edu.cn

[*]vrstamenkovic@anl.gov

[*]ydli@mail.tsinghua.edu.cn

[▽]H.D., D.L. and Y.T. contributed equally.

## Table of Contents

## Supplementary Figures

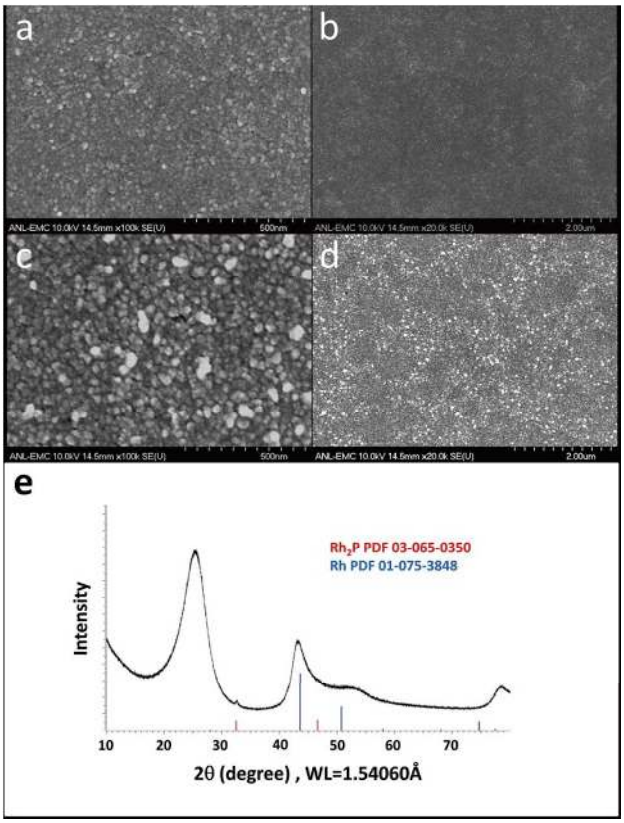


**Figure S1.** SEM images of the (a),(b) Rh and (c),(d) $Rh_2P$ thin films. (e) XRD pattern of $Rh_2P$ thin film.

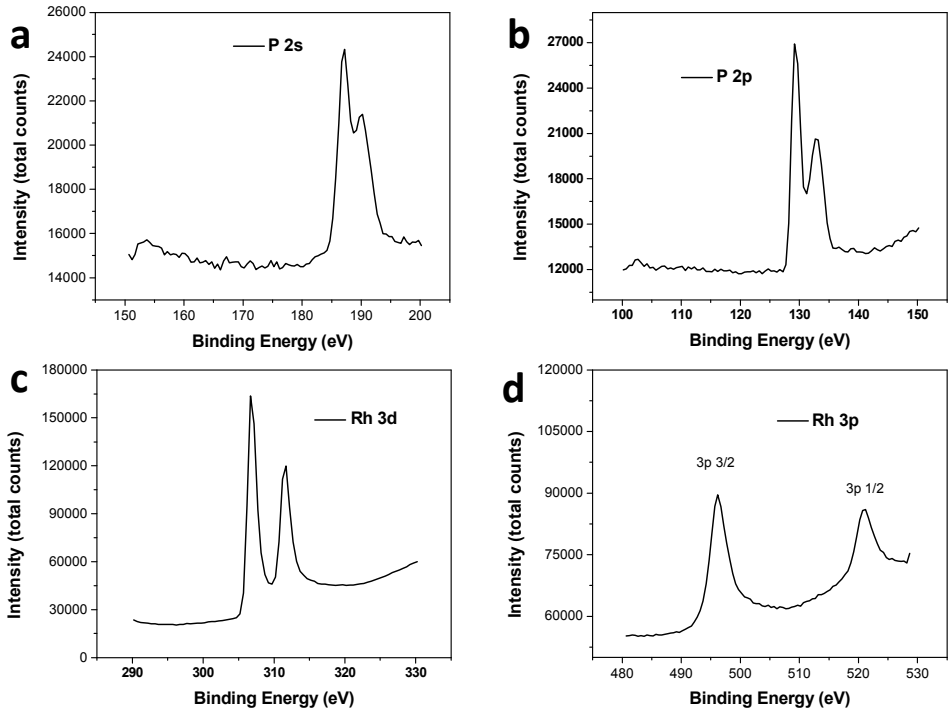


**Figure S2.** XPS spectra for $Rh_2P$ thin films.* (a) Phosphorus 2s, 129.2 eV ($Rh_2P$), 132.7 eV (P oxide). (b) Phosphorus 2p, 187.2 eV ($Rh_2P$), 190.2 eV (P oxide). (c) Rhodium 3d, 306.7 eV (pure Rh), 311.7 eV ($Rh_2P$). (d) Rhodium 3p, 3p1/2, 520.7 eV ($Rh_2P$), 3p3/2, 496.2 eV (pure Rh). (*NIST X-ray Photoelectron Spectroscopy Database, NIST Standard Reference Database 20, Version 4.1 https://srdata.nist.gov/xps/)

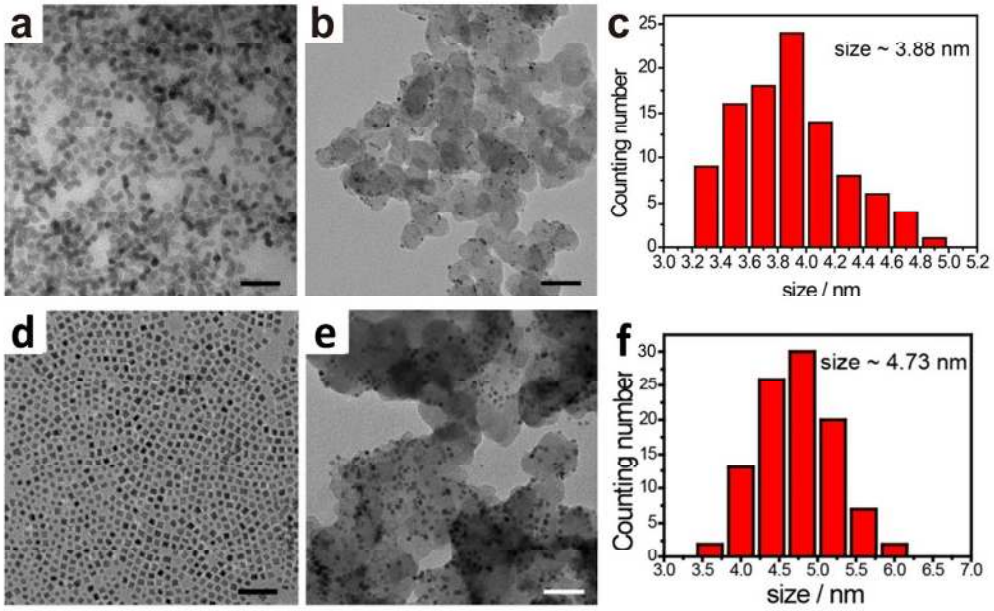


**Figure S3.** Characterizations of Rh NCs and $Rh_2P$ NCs. (a-c) TEM images of as-synthesized Rh NCs (scale bar, 20 nm), Rh NCs supported on Vulcan XC-72 carbon (scale bar, 50 nm) and size distribution of Rh NCs, respectively. (d-f) TEM images of as-synthesized $Rh_2P$ NCs, $Rh_2P$ NCs supported on Vulcan XC-72 carbon and size distribution of $Rh_2P$ NCs, respectively. Scale bar equals 50 nm.

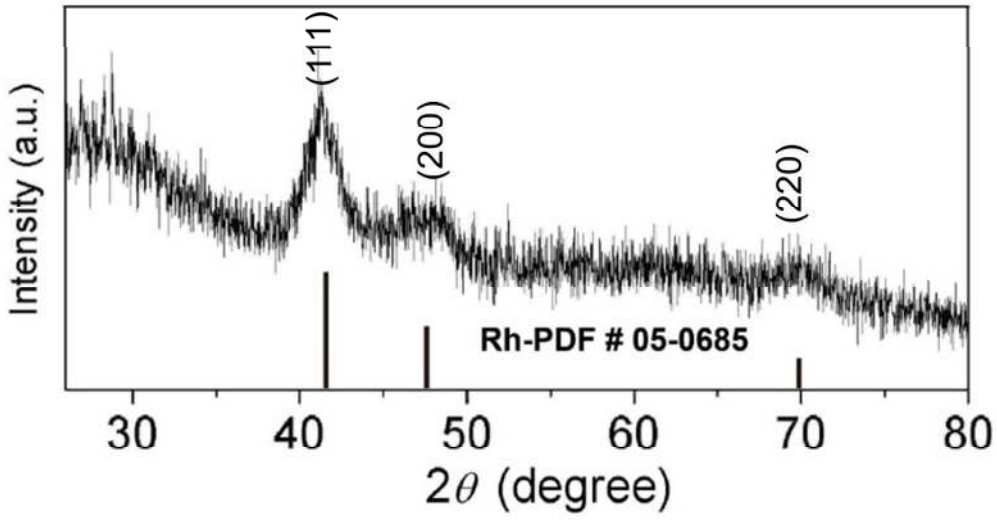


**Figure S4.** XRD pattern of Rh NCs. XRD pattern of Rh NCs (up) and metallic Rh (bottom, JCPDS: 05-0685).

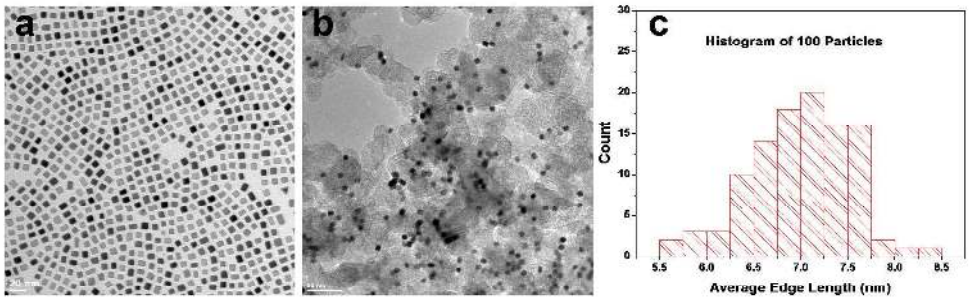


**Figure S5.** (a) TEM image of as-synthesized Pt nancubes. Scale bar equals 20 nm. (b) TEM image of Pt nanocubes loaded on Vulcan XC-72 carbon after annealing at 185 °C in air. Scale bar equals 50 nm. (c) Histogram of particle size distribution counted from 100 particles. Average particle edge length is 7.0 nm ± 0.6 nm.

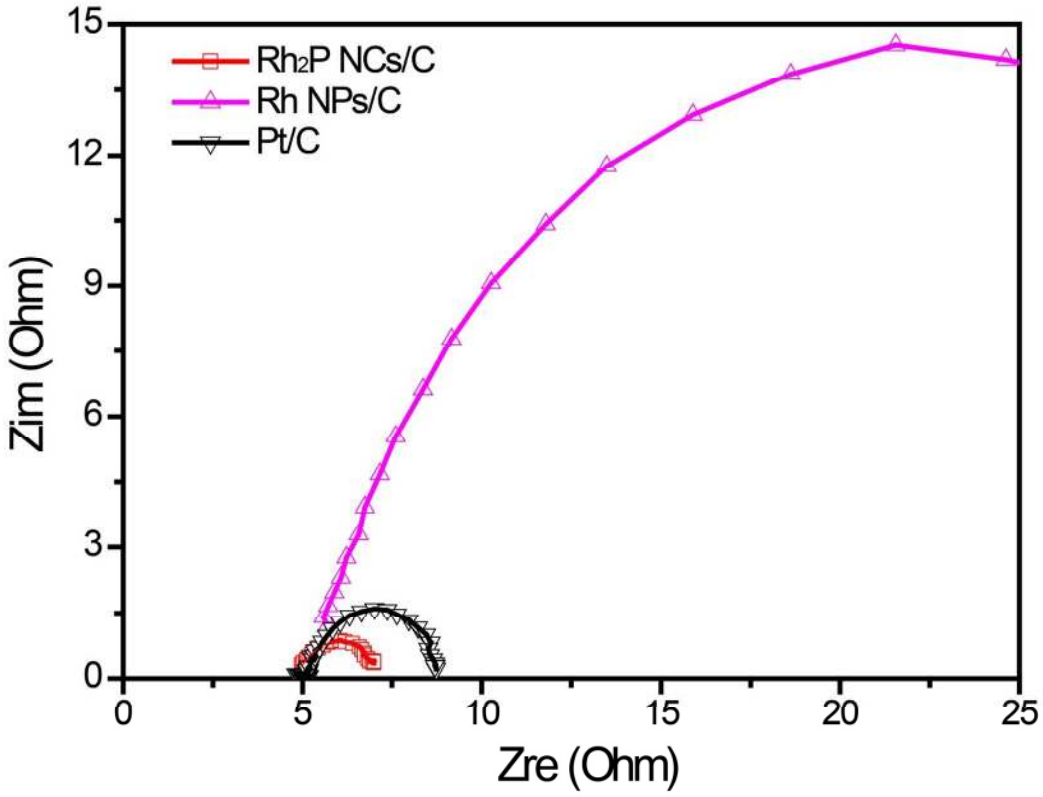


**Figure S6.** Nyquist plots of comparing catalysts. Nyquist plots under η = 3.8 mV.

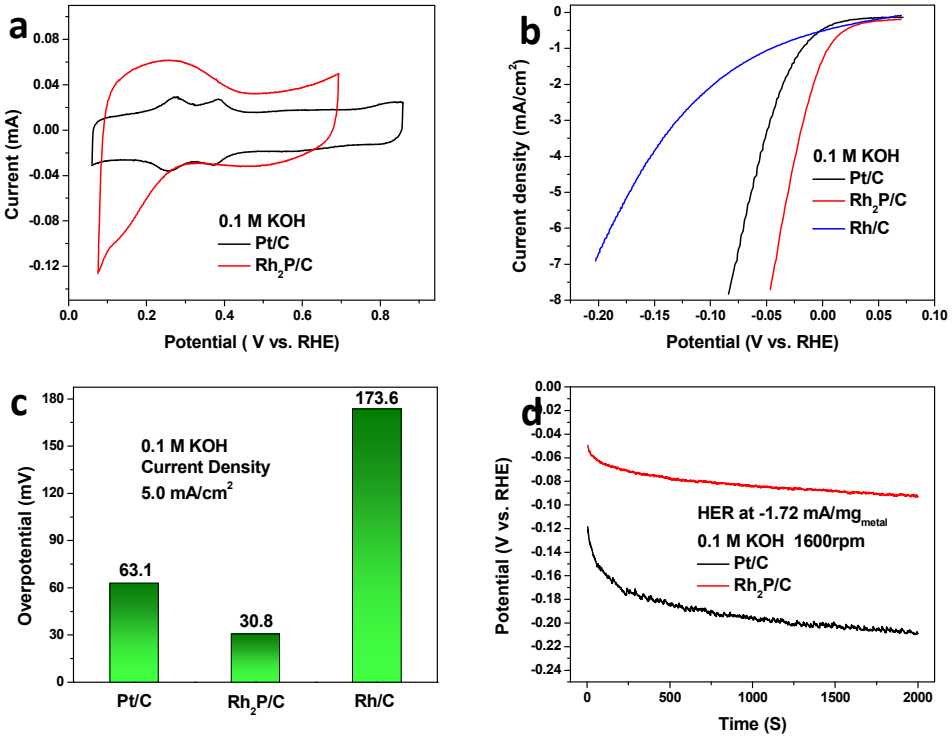


**Figure S7.** Hydrogen evolution reaction properties in alkaline media (0.1 M KOH). (a) Cyclic voltammograms of $Rh_2P$/C and Pt/C. (b) Polarization curves for Pt/C (3.7 $\mu g_{Pt}/cm^2$), $Rh_2P$/C (3.7 $\mu g_{Rh}/cm^2$) and Rh/C (13.3 $\mu g_{Rh}/cm^2$) recorded at 20 mV/s and (c) Corresponding overpotentials at 5.0 $mA/cm^2$ current density. (d) Chronopotentiometry of the $Rh_2P$/C and Pt/C recorded at -1.72 $mA/mg_{metal}$ current density. The potentials were converted to RHE and corrected for iR drop.

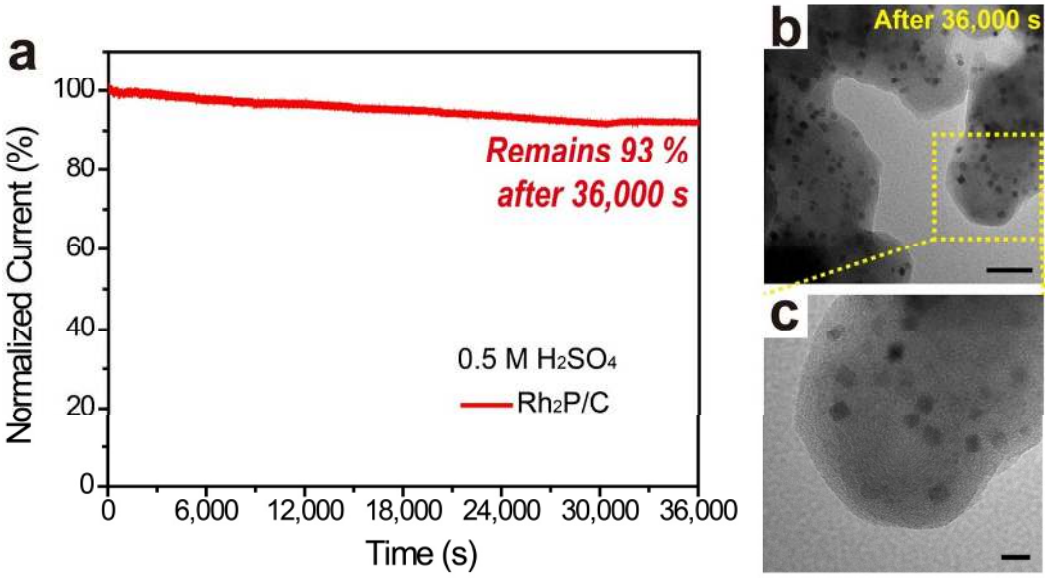


**Figure S8.** Durability performance of the $Rh_2P$ catalyst. (a) Chronoamperometry for $Rh_2P$/C under overpotential $\eta$ = 109 mV for 36,000 s, showing electrochemical durability under acidic conditions (0.5 M $H_2SO_4$). (b) Low-magnification (scale bar, 40 nm) and (c) high-magnification (scale bar, 10 nm) TEM images of $Rh_2P$/C after electrolysis for 36,000 s.

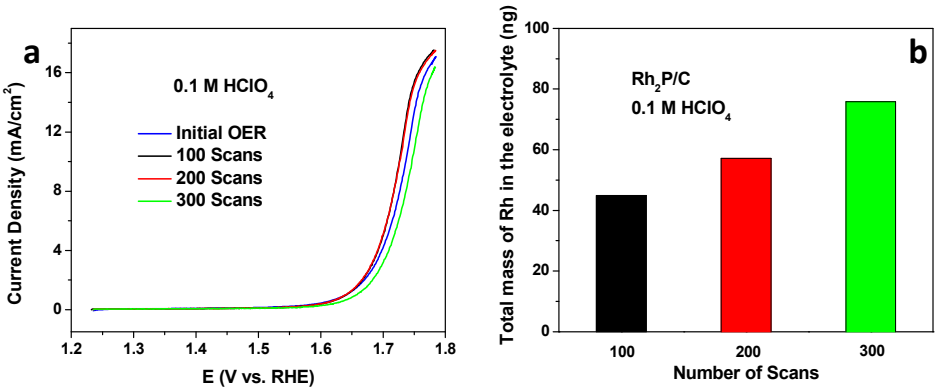


**Figure S9.** $Rh_2P$/C OER stability under potential cycling. (a) Polarization curves for $Rh_2P$/C recorded at 20 mV/s, 1600 rpm, 0.1 M perchloric acid. (b) Total mass of Rh (nanograms) in the electrolyte from ICP analysis. The potential cycling was between 1.23 V and 1.78 V, at the scan rate of 50 mV/s.

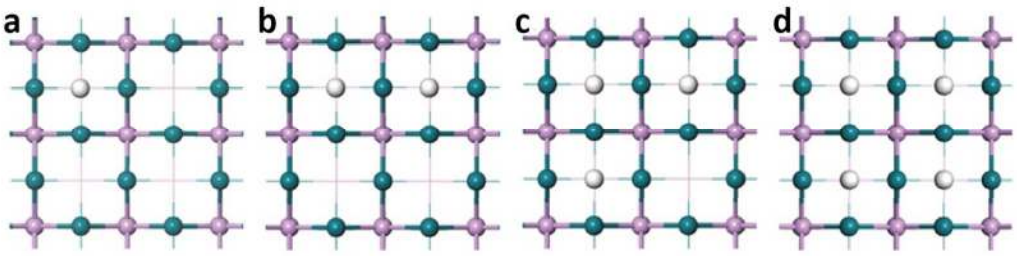


**Figure S10.** Optimized structures of H adsorption with different coverage on Rh-terminated surface.

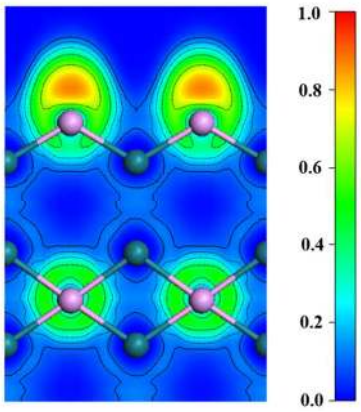


**Figure S11.** Calculated electron localization function (ELF) of the $Rh_2P$ (200) surface. The calculated ELF value ranges from 0.0 (blue) to 1.0 (red).

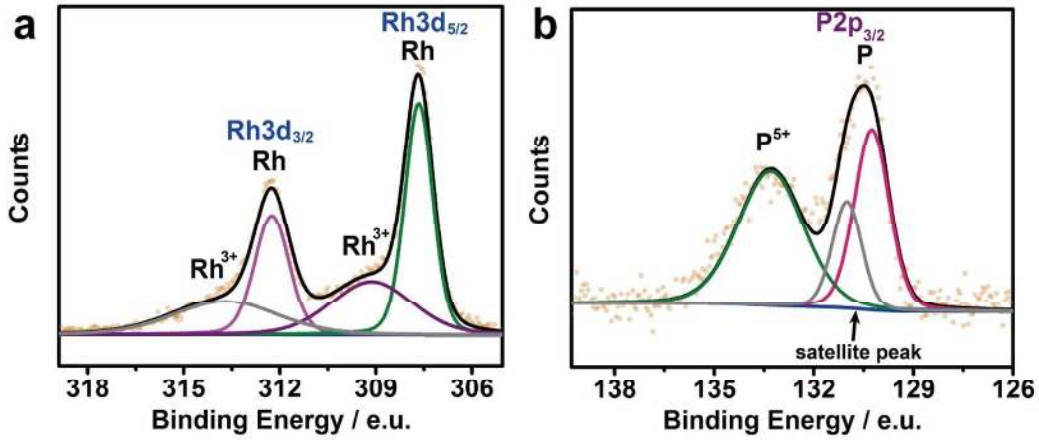


**Figure S12.** XPS spectra for $Rh_2P$/C. XPS spectra in the (a) Rh(3d) regions and (b) P(2p) region of AA washed $Rh_2P$/C.

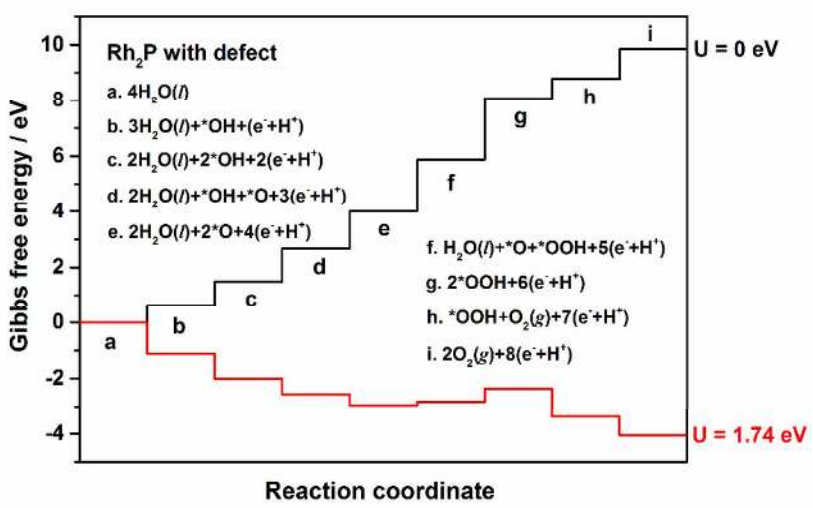


**Figure S13.** Gibbs free energy profiles. The calculated Gibbs free energy profiles of the intermediate states in OER on $Rh_2P$ (200)-defect surface.

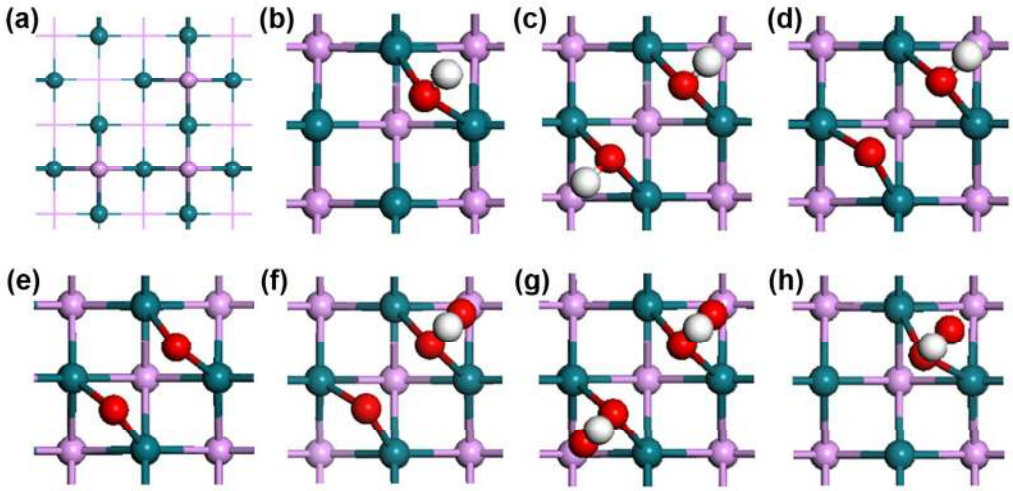


**Figure S14.** Optimized structures of the intermediate states in OER on $Rh_2P$ (200)-defect surface. (a) Optimized structures of the $Rh_2P$ (200) surface with defect. (b-h) Optimized structures of the intermediate states in OER on $Rh_2P$ (200)-defect surface.

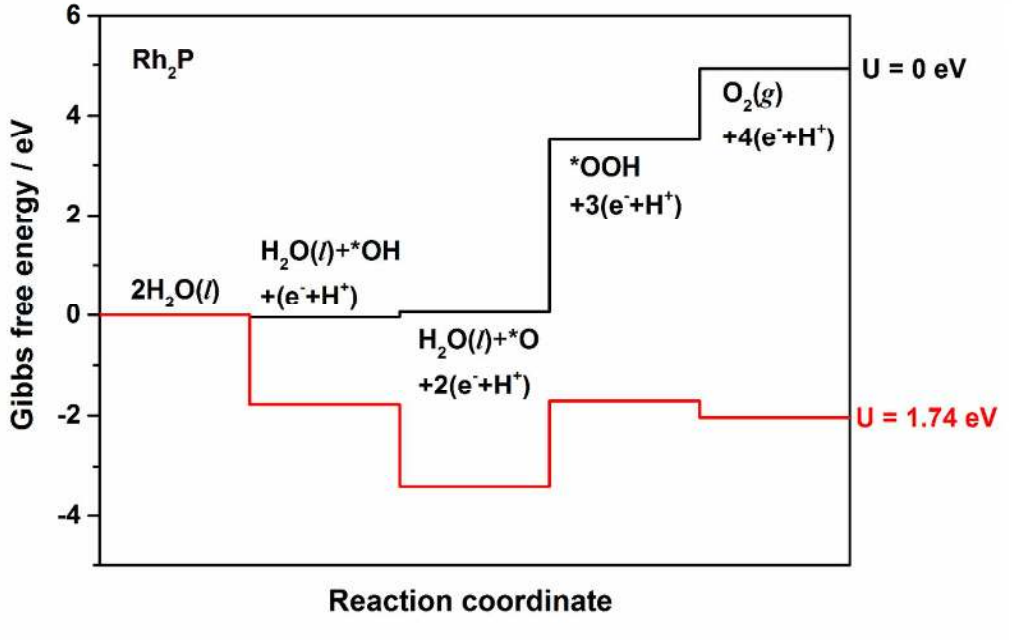


**Figure S15.** Gibbs free energy profiles. The calculated Gibbs free energies (eV) profiles of the intermediate states in OER on $Rh_2P$ (200) surface.

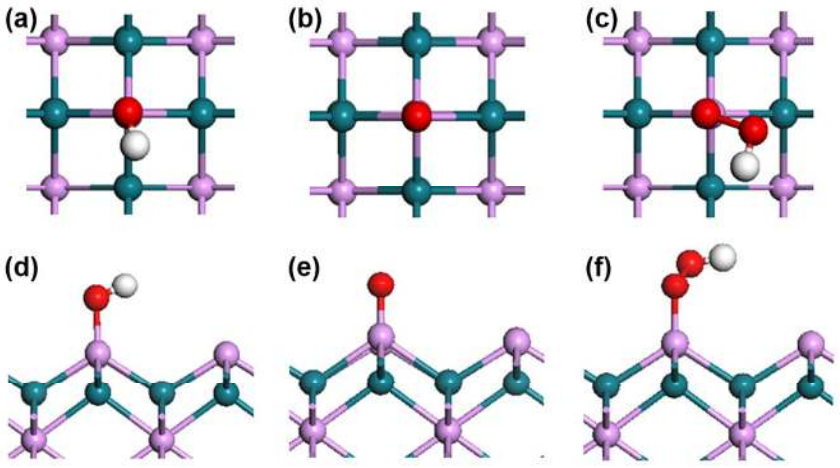


**Figure S16.** Optimized structures of the intermediate states in OER on $Rh_2P$ (200) surface. (a) and (d) are the top view and side view of the *OH; (b) and (e) are the top view and side view of the *O; (c) and (f) are the top view and side view of the *OOH.

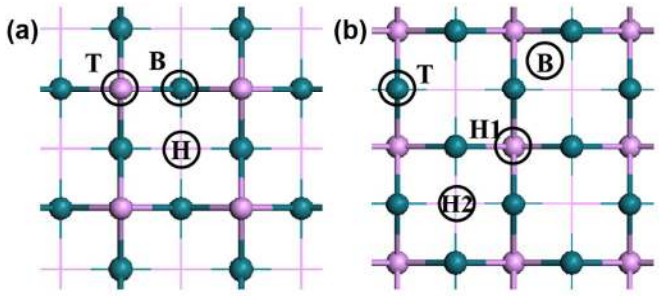


**Figure S17.** Binding sites of H atom. The binding sites for H adsorption on the top view of (a) P-terminated and (b) Rh-terminated $Rh_2P$ (200) surfaces.

## Supplementary Tables

**Table S1. ICP-AES analysis.**

| Materials | Rh (μg/mL) | P (μg/mL) | Rh / P (mmol/mmol) |
|---|---|---|---|
| $Rh_2P$ NCs/C (not treated by AA) | 136.7 | 24.9 | 1.65 |
| $Rh_2P$ NCs[1]/C | 132.9 | 18.6 | 2.15 |

[1]The materials were washed with AA by using method described in experimental section.

**Table S2. Calculated adsorption energies and Gibbs free energies of H adsorption on $Rh_2P$ (200) surfaces**.

| H coverage | P−terminated | | Rh−terminated | |
|---|---|---|---|---|
| | $\Delta E_H$ (eV) | $\Delta G°_H$ (eV) | $\Delta E_H$ (eV) | $\Delta G°_H$ (eV) |
| 1/4 ML | -0.08 | 0.15 | -0.58 | -0.51 |
| 2/4 ML | -0.25 | 0.00 | -0.66 | -0.51 |
| 3/4 ML | -0.05 | 0.18 | -0.84 | -0.66 |
| 4/4 ML | -0.06 | 0.17 | -0.90 | -0.75 |

**Table S3. Calculated Free Energies of Reaction Steps in OER on $Rh_2P$ (200)-defect Surface.**

| steps | $\Delta E$ | $\Delta_{0\rightarrow 298K}\Delta H$[ab] | $\Delta ZPE$ | $-T\Delta S$[bc] | $-\|e\|U$ | $\Delta G$ |
|---|---|---|---|---|---|---|
| $H_2O \rightarrow *OH+e^-+H^+$ | 0.29 | -0.06 | -0.08 | 0.47 | -1.74 | -1.12 |
| $H_2O \rightarrow *OH+e^-+H^+$ | 0.50 | -0.06 | -0.06 | 0.47 | -1.74 | -0.89 |
| $*OH \rightarrow *O+e^-+H^+$ | 1.52 | 0.04 | -0.17 | -0.2 | -1.74 | -0.55 |
| $*OH \rightarrow *O+e^-+H^+$ | 1.67 | 0.04 | -0.18 | -0.2 | -1.74 | -0.41 |
| $H_2O+*O \rightarrow *OOH+e^-+H^+$ | 1.52 | -0.06 | -0.06 | 0.47 | -1.74 | 0.13 |
| $H_2O+*O \rightarrow *OOH+e^-+H^+$ | 1.87 | -0.06 | -0.08 | 0.47 | -1.74 | 0.47 |
| $*OOH \rightarrow O_2+e^-+H^+$ | 1.61 | 0.13 | -0.21 | -0.83 | -1.74 | -1.03 |
| $*OOH \rightarrow O_2+e^-+H^+$ | 1.95 | 0.13 | -0.19 | -0.83 | -1.74 | -0.68 |

a. $\Delta_{0\rightarrow 298K}\Delta H$ denotes the correction of $\Delta H$ from 0K to 298K.

b. These data were cited from D.R. Stull, H. Propher, JANAF Thermochemical Tables, U. S. National Bureau of Standards, Washington, DC, 1971.

c. The value of $T\Delta S$ ($H_2O$) includes the correction of $\Delta G$ ($H_2O$) from gas to liquid.

**Table S4. Calculated Free Energies of Reaction Steps in OER on $Rh_2P$ (200) Surface.**

| steps | $\Delta E$ | $\Delta_{0\rightarrow 298K}\Delta H$ | $\Delta ZPE$ | $-T\Delta S$ | $-\lvert e\rvert U$ | $\Delta G$ |
|---|---|---|---|---|---|---|
| $H_2O \rightarrow *OH + e^- + H^+$ | -0.36 | -0.06 | -0.09 | 0.47 | -1.74 | -1.78 |
| $*OH \rightarrow O* + e^- + H^+$ | 0.39 | 0.04 | -0.13 | -0.2 | -1.74 | -1.64 |
| $H_2O + *O \rightarrow *OOH + e^- + H^+$ | 3.14 | -0.06 | -0.10 | 0.47 | -1.74 | 1.71 |
| $*OOH \rightarrow O_2 + e^- + H^+$ | 3.46 | 0.14 | -0.19 | -0.83 | -1.74 | -0.33 |

**Table S5. Calculated binding energies (eV) of one H atom on $Rh_2P$ (200) surfaces**

| Binding site | Binding energy (eV) | |
|---|---|---|
| | P-terminated | Rh-terminated |
| top (T) | -0.07 | -0.21 |
| bridge (B) | 0.63 | -b |
| hollow1 (H1) | 0.78[a] | -c |
| hollow2 (H2) | 0.78[a] | -0.58 |

a For P-terminated $Rh_2P$ (200) surface, hollow1 and hollow2 site are the same

b The adsorption on the bridge site is unstable and the H atom moves to the hollow2 site

c The adsorption on the hollow1 site is unstable and the H atom moves to the hollow2 site